

FATIGUE BEHAVIOR OF SELECTIVE LASER MELTED 17-4 PH STAINLESS STEEL

Aref Yadollahi¹, Nima Shamsaei^{1,*}, Scott M. Thompson¹, Alaa Elwany², Linkan Bian³
& Mohamad Mahmoudi²

¹Department of Mechanical Engineering, Mississippi State University, Mississippi State, MS
39762

¹Center for Advanced Vehicular Systems (CAVS), Mississippi State University, Mississippi
State, MS 39762

²Department of Industrial and Systems Engineering, Texas A & M University, College Station,
TX

³Department of Industrial and Systems Engineering, Mississippi State University, Mississippi
State, MS 39762

*Corresponding author:

Email: shamsaei@me.msstate.edu

Phone: (662) 325 2364

REVIEWED

Abstract

In this investigation, fully-reversed strain-controlled fatigue tests were conducted on Selective Laser Melted (SLM) 17-4 PH stainless steel (SS). Cylindrical 17-4 PH rods were fabricated vertically-upward using optimized process parameters to ensure a dense product. Post-fabrication heat treatments (solution annealing and aging) were applied on half of the as-built samples. Fatigue behavior and tensile properties of the as-built and heat treated samples were investigated and compared with available data from the literature. The microstructure analysis and fractography were performed to discern the failure initiation sites, crack propagation path, and fracture surface morphology. Fatigue lives of SLM 17-4 PH SS specimens were found to be significantly shorter than their wrought counterparts. It was also found that heat treatment hardens the SLM 17-4 PH SS specimens while also shortens their fatigue life in the high cycle regime. The presence of defects, which serve as crack initiation sites, and more sensitivity of heat treated specimens to impurities, due to higher hardness, were the main reasons for these observations.

Introduction

During the past decade, increasing attention has been drawn to additive manufacturing (AM), a unique manufacturing process in which a part is built up layer-by-layer in contrast to traditional, ‘subtractive’ metalworking processes. Additive manufacturing is currently demonstrating its proficiency in fabricating components with sophisticated geometries targeted towards biomedical, aerospace, and defense industries [1]. Of the AM techniques available, Selective Laser Melting (SLM), which is a laser based powder bed system, provides a means to obtain relatively fine surface quality, high precision, powder efficiency, etc. For a typical SLM process, a thin layer of metallic powder is placed on the substrate and a focused laser follows a pattern over the surface, melting powder particles to form a part layer by layer. The build process is conducted in an inert atmosphere (e.g. argon).

Fabricating AM components with microstructural and mechanical properties comparable to those produced by conventional manufacturing techniques is still a major challenge. This is due to the many involved process parameters (such as: laser power, beam travel speed, layer thickness, scanning strategy, part building orientation) providing for complex thermal histories that then lead to the formation of a non-homogeneous, anisotropic microstructure with inevitable porosity [2]. In general, static mechanical properties (such as tensile, compression, hardness, etc.) of AM parts are comparable or even higher than those of wrought and cast materials due to relatively high cooling rates experienced during fabrication which favors the production of finer microstructures. However, lower fatigue strength has been reported for AM parts due to detrimental effects caused by defects such as pores and inclusions - inherent consequences of many powder-based AM techniques. Thus, finding effective optimization and control mechanisms to fabricate components via AM with superior mechanical properties is of interest [3].

Among the many steels that have been processed with SLM, precipitation hardened (PH) steels are more attractive due to their weldability and austenitic/martensitic microstructure [4]. These alloys have been used for structures in nuclear, aerospace, marine, naval, and chemical industries [5,6]. Stainless steel 17-4 PH is one of the most popular alloys in this category due to its relatively high tensile/impact strength, fracture toughness and corrosion resistance at typical service temperatures below 300 °C [7].

Microstructural and mechanical properties of SLM 17-4 PH SS have been reported and discussed in the literature [8–11], and the high cycle fatigue behavior of both additively- and conventionally-manufactured 17-4 PH SS under stress-control tests has been investigated extensively [5,10,12]. However, to the best of authors’ knowledge, there is no available report on the strain-controlled low cycle fatigue behavior of this material. Therefore, the aim of this study is to investigate strain-controlled fatigue behavior of SLM 17-4 PH SS. The effect of an appropriate heat treatment (solution annealing and aging) on fully-reversed fatigue strength of SLM 17-4 PH SS is also studied. Fatigue fracture surfaces are also examined using Scanning Electron Microscopy (SEM) to capture the crack initiation site, crack propagation and failure mechanisms involved.

Experimental Procedures

Commercially-procured, gas-atomized 17-4 PH SS powder (Phenix Systems), with 80 percent of its size distribution falling below 22 μm, was utilized for fabricating rods via a SLM machine (ProX™ 100). Process parameters (i.e. laser power, scanning speed, layer thickness, and hatching pitch) were selected to obtain an acceptable level of final part density using a sequential experimental methodology [13]. Utilized process parameters (i.e. laser power, scanning speed, layer thickness, and hatching pitch) are summarized in Table 1.

Table 1. Utilized SLM process parameters for fabricating 17-4 PH SS rods.

Laser Power (W)	Scanning Speed (mm/s)	Hatching Pitch (μm)	Layer Thickness (μm)
48	300	50	30

Cylindrical rods, with 8 mm diameter and 75 mm height, were fabricated upward in a vertical orientation on a base plate. After fabrication, the specimens were removed from the base plate via Electrical Discharge Machining (EDM). In order to investigate the effect of heat treatment, half of the as-built samples were subjected to solution annealing for 30 min at approximately 1040 °C followed by air cooling (AC) to room temperature (Condition A) and then, these same samples underwent precipitation hardening for 1 hour at 482°C followed by AC to room temperature (Condition H900). It has been reported that when subjecting as-built SLM 17-4 PH SS samples to direct aging, age hardening will not occur due to the presence of dual phase microstructure (i.e. martensitic and austenitic phases) [8]. Therefore, solution annealing was performed on the as-built samples before peak-aging. Heat treated and non-heat-treated tensile and fatigue tests specimens were machined from the SLM samples to the configuration and dimensions in conformance to the ASTM E466 standard [14], as shown in Fig. 1. After machining, the specimens were polished to a roughness of $R_a < 0.7 \mu\text{m}$ in order to minimize surface defects. The polished specimen roughness was determined using a non-contact (i.e. laser reflectance) measurement system (Talysurf).

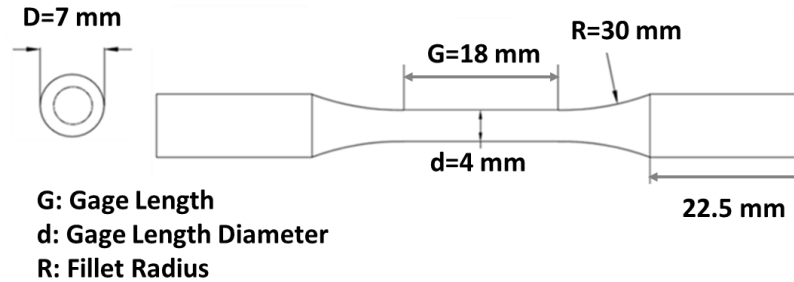


Figure 1. Dimensions of fatigue and tensile specimens according to ASTM E 606 [14].

Tension experiments were conducted at room temperature using an Instron 5882 servo-hydraulic testing machine with a ± 100 kN maximum loading capacity at a 0.001/s nominal strain rate. Fully-reversed strain-controlled fatigue tests, with a strain ratio of $R = -1$, were performed with an MTS Tabletop 858 machine under various strain amplitudes. Fatigue experiments were performed in accordance with ASTM E606 under a sinusoidal loading waveform until failure occurred or 10^6 cycles was reached, in which the test was considered to be a run-out. Fatigue test frequencies were adjusted according to strain amplitude. One specimen from each set was mounted and etched for microstructural characterization using optical microscopy (OM) (ZEISS Axiovert 200). Fracture surfaces of fatigued specimens were Au/Pd sputter-coated and examined using scanning electron microscopy (SEM) (FEG SEM Zeiss SUPRA™ 40) to determine crack initiation site and crack propagation characteristics.

Results and Discussions

Microstructure

The microstructure of SLM parts depends primarily on the temperature gradients and cooling rates (i.e. thermal history) experienced during the manufacturing process. The utilized process parameters will directly impact the heat transfer into the powder bed, and this will then affect the generated melt pool size, heat affected zone (HAZ), and cooling rate [11]. The heat-

dependent, encumbered microstructure of SLM parts is of importance as it will impact their mechanical properties.

Optical micrographs of the longitudinal cross-section of SLM 17-4 PH SS samples, in the as-built and heat treated conditions, are shown in Figs. 2(a) and (b), respectively. The microstructural examination revealed the presence of voids; including pores due to entrapped gas and un-melted regions between layers due to insufficient fusion combined with low laser penetration depth. Such defects can impact the mechanical properties of the material, especially elongation to failure and fatigue behavior. It was also found that post-manufacturing heat treatment has a substantial impact on the microstructure. After solution annealing and peak-aging, the microstructure transformed to a fully recrystallized structure, as presented in Fig. 2(b). Precipitation at grain boundaries during the peak-aging treatment can be clearly seen in Fig. 2(b), since these regions were easier to be etched. Heat treatment, as expected, homogenized the microstructure as compared to the non-heat-treated samples, as shown in Fig. 2(a). In addition, it can be observed that heat treatment eradicates interfacial regions between deposited layers.

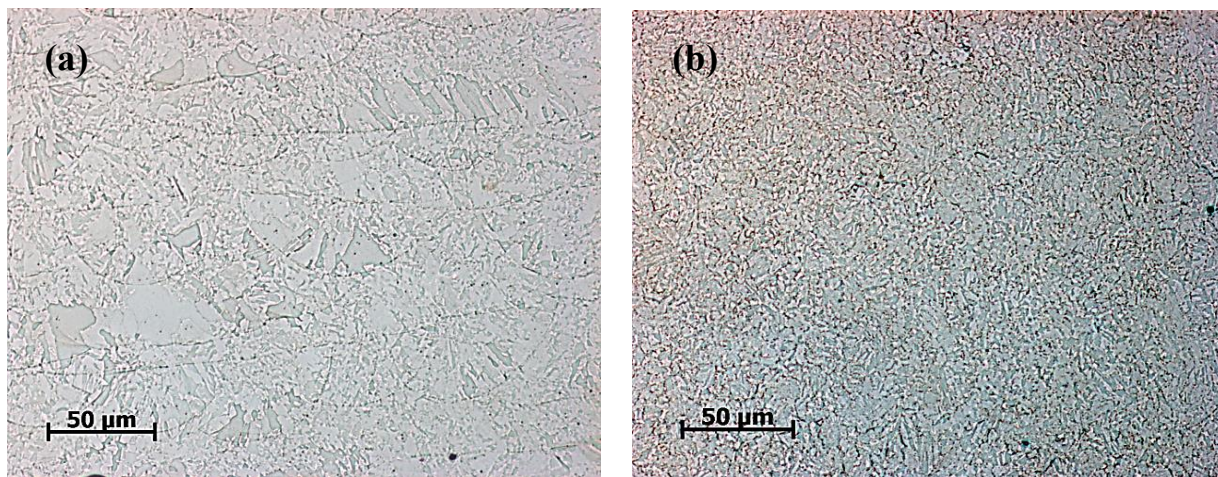


Figure 2. Longitudinal cross-section images of SLM 17-4 PH SS in (a) as-built and (b) heat treated conditions.

Tensile Properties

Tensile properties of the heat treated and non-heat-treated SLM 17-4 PH SS are presented in Fig. 3. As shown, the yield and ultimate tensile strengths are significantly increased after heat treatment (solution annealing and aging), but elongation to failure is reduced. This behavior is due to precipitation hardening of the chromium-nickel-copper constituents which prevents dislocation movement causing metal to resist deformation and become harder [15]. The monotonic tension results reveal that the yield and ultimate tensile strengths of SLM 17-4 PH SS in as-built condition are lower than those of wrought material in H900 condition (yield stress: 1,170 MPa, ultimate tensile stress: 1,310 MPa) [16]. This is due to the fact that the SLM 17-4 PH SS samples are not completely martensitic, but contain retained austenite due to high solidification speeds during fabrication, which prevent the formation of the martensite phase in the as-built material, leading to a metastable austenitic microstructure. The presence and amount of retained austenite may have a significant influence on the material's strength, strain hardening and elongation to failure [6,8]. Therefore, a post-manufacturing heat treatment is necessary to

enhance the mechanical properties of SLM 17-4 PH SS. The yield and ultimate tensile strengths of heat treated SLM 17-4 PH SS is comparable to those of conventionally-manufactured parts in the H900 condition. However, elongation to failure of heat treated specimens is noticeably lower than wrought materials in the H900 condition (10% elongation to failure). Lower ductility of SLM 17-4 PH SS is attributed to the presence of defects, such as pores and un-melted powder, resulting from entrapped gas and/or lack of fusion during fabrication.

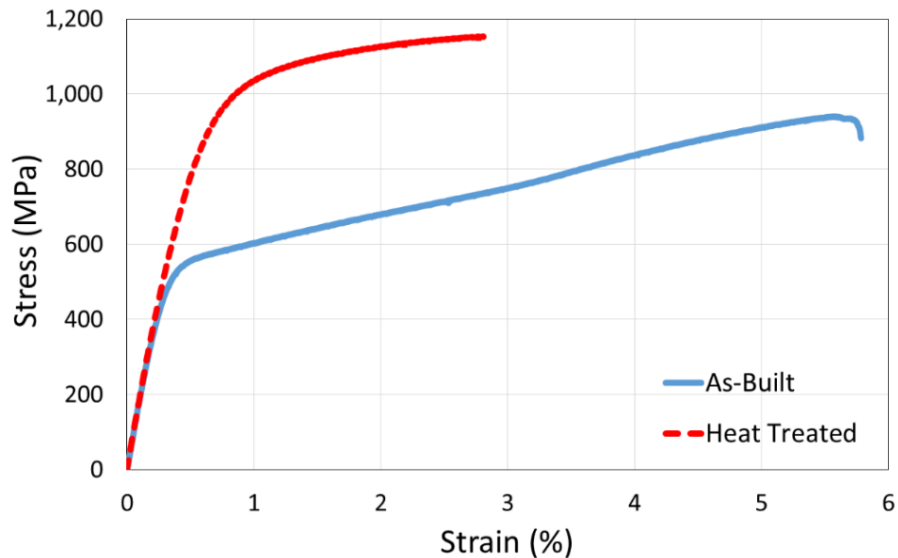


Figure 3. Engineering stress-strain curves of SLM 17-4 PH SS in as-built and heat treated conditions.

Fatigue Behavior

Fatigue is the main mechanical failure mode for most components and structures. Unlike failure due to sudden or monotonic loads, fatigue is a localized and microstructural-dependent failure mode resulting from cyclic loading over longer time scales. In fact, fatigue failure, as a result of cyclic loading, can occur due to a stress that is much lower than failure-causing monotonic stress. The three characterized stages of fatigue failure are: crack initiation (nucleation), crack propagation and final fracture – all corresponding to categorized regions of fatigue fracture surfaces. Generally, cracks tend to initiate from microstructural defects (i.e. pores and particles) and grain boundaries. However, in the case of AM/SLM parts, defects can be the main source of crack initiation [3]. These features may create local microscopic stresses larger than the yield strength, causing local plastic deformation and leading to fatigue crack initiation under cyclic loading.

Fatigue life is typically quantified by the number of load cycles/fluctuations until failure, N_f . Generally speaking, fatigue life that is less than 10^3 cycles is considered as low cycle fatigue (or short-life regime), fatigue life in the range of $10^3 < N_f < 10^5$ is classified as mid-cycle fatigue (or mid-life regime), and $N_f > 10^5$ is categorized as high-cycle fatigue (or long-life regime). The most commonly used fatigue life models (to predict N_f) are the nominal stress-life ($S - N$) model and the local strain-life ($\epsilon - N$) model. The stress-life method is traditionally used for the fatigue life analysis at the high cycle fatigue (HCF) regime. This method relates the nominal stresses to local fatigue strengths. The strain-life method involves a more thorough

analysis of the plastic deformation at localized regions, and consequently, can better characterize the fatigue behavior of a material, specifically in the presence of plastic deformations - making it the most appropriate for low cycle fatigue (LCF) applications.

The results of uniaxial fully-reversed ($R = -1$) fatigue tests of SLM 17-4 PH SS, performed at various strain amplitudes, are illustrated as $(\epsilon - N)$ curves in Fig. 4. For a more conservative estimation, the run-out specimens were not considered for curve fitting. The scatter in results was greatest for tests conducted in longer life regimes and least for tests conducted at shorter life regimes. This is due to the fact that defect size and location (i.e. distance from surface) significantly affects the fatigue life in the HCF regime, where crack initiation constitutes a dominant part of total life. As shown in Fig. 4, the heat treated SLM specimens demonstrate higher fatigue strengths relative to their as-built counterparts in LCF, but the opposite trend occurs for HCF. The behavior of heat treated SLM specimens in HCF contrasts the expectation that the high cycle fatigue strength of steel typically increases with an increase in tensile strength [17].

It is well known that crack initiation dominates total fatigue lifetime in HCF [18]. Therefore, it is expected that the heat treated SLM specimens exhibit more HCF life as compared to their as-built counterparts - since they possess higher strength and more resistance to dislocation movement within the matrix, both resulting in enhanced resistance to crack initiation. Moreover, coherent copper-rich precipitates in the matrix of the peak-aged (H900 condition) specimens are expected to provide more resistance to crack initiation. However, this is not the case for AM specimens that already contain defects as large as $100 \mu\text{m}$ in some cases. Therefore, defect size, shape, and location may play a more dominant role in HCF life of AM/SLM parts. In addition, heat treated specimens are harder, and therefore, more sensitive to impurities, specifically in HCF regime.

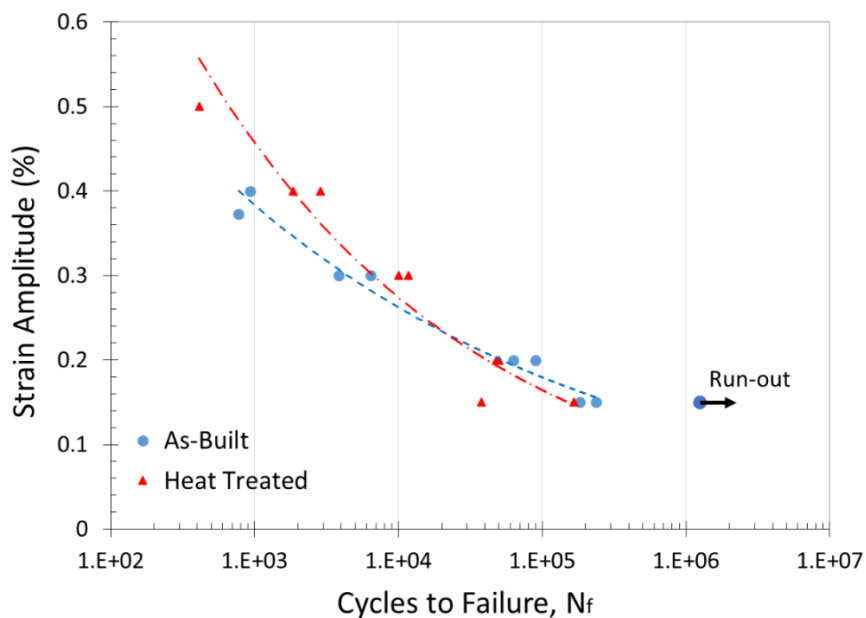


Figure 4. Strain-life fatigue experimental data and curves for SLM 17-4 PH SS in both as-built and heat treated conditions.

Maximum stress-life fatigue data of heat treated SLM 17-4 PH SS and their comparison with wrought material in the H1050 condition [19] is presented in Fig. 5(a). The fatigue stress amplitude versus life of SLM 17-4 PH SS (in the as-built condition) is also compared with reported performance data for as-built Direct Metal Laser Sintered (DMLS) 17-4 PH SS [10] in Figure 5(b). The fatigue data for wrought material (H1050 condition) reported in Fig. 5(a) belong to the flat specimens ($K_T = 1$) tested under completely reversed axial loading ($R = -1$) [19]. The fatigue data reported in Figure 5(b) belong to DMLS horizontally-built specimens tested using a rotating bending testing machine ($R = -1$) [10]. The surface of each specimen was polished in both studies. Although general observations are warranted, there is inadvertent variance in fatigue data due to different testing modes, specimen types, load setups, fabrication processes, etc.; hence, it is difficult to make direct comparisons between results from this study and others in literature.

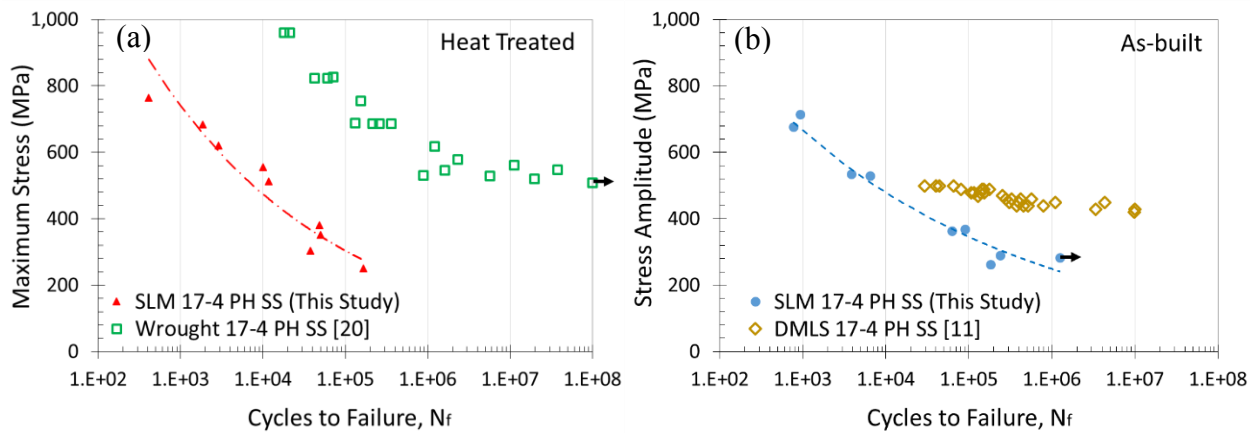


Figure 5. Comparison of fatigue stress life data (a) for heat treated SLM 17-4 PH SS (this study) to wrought 17-4 PH SS in H1050 condition from [19] and (b) for as-built SLM 17-4 PH SS (this study) to DMLS 17-4 PH SS in as-built condition from [10].

As shown in Figure 5(a), SLM 17-4 PH SS demonstrates significantly shorter fatigue lives as compared to the wrought material in the H1050 condition. This is attributed to the presence of a large number of defects including pores, un-melted regions, and un-melted powder particles which serve as crack initiation sites. Moreover, the ultimate tensile property reported by Leybold [19] (1,414 MPa) is significantly higher than those measured for the heat treated SLM 17-4PH SS in this study. From Figure 5(b), it can be seen that the mid and high cycle fatigue strength of the as-built SLM 17-4 PH SS is also lower than the DMLS data reported by Sehart and Witt [10]. This can be due to differences in (1) building orientation (i.e. vertical in this study versus horizontal in Sehart and Witt [10]) and (2) utilized process parameters which affect the thermal histories during fabrication, and consequently, microstructure and phase proportion of the material. Furthermore, a rotating bending test may be less severe than a uniaxial tensile fatigue tests (employed in this study), since the whole gage section is subjected to the maximum stress for the latter, while only portions of the gage surface experiences the maximum stress under rotating bending. Statistically, more impurities can serve as the crack initiation site in closed loop uniaxial fatigue machine as compared to the rotating bending test where less volume and impurities are exposed to maximum stress.

Fractography

The analysis of the fatigue fracture surfaces of the heat treated and non-heat-treated SLM 17-4 PH SS specimens reveals that crack initiations occur at defects adjacent to specimens' surface, including pores due to entrapped gas, and un-melted regions (or weak metallurgical bounding between layers) resulting from lack of fusion (or low penetration depth of laser). This indicates that although machining and polishing reduces the surface roughness (due to partially-melted powder particles and the inconsistency of melt pool) and associated notch effects, remnant interior pores and sub-surface defects that are brought to the surface still play a dominant role in crack initiation. Scatter in fatigue life data have a direct relationship with size and location (i.e. distance from surface) of pores and un-melted regions. Larger un-melted regions and/or ones closer to the surface have more detrimental effects on fatigue strength, especially during HCF. For specimens that failed relatively early (in HCF), larger un-melted regions have been detected near the specimens surface.

Figure 6(a) demonstrates a typical fatigue fracture surface of an as-built SLM specimen that failed in the long life regime (i.e. low strain amplitude). As shown in Fig. 6(b), an un-melted region close to the specimen surface acts as a stress raiser and serves as a site for crack initiation. However, multiple crack initiation sites were found on the fracture surface of specimens tested in the short life regime, as depicted in Fig. 7(a). As can be seen in Figs. 7(b) and (c), for a specimen tested in LCF, cracks appear to have initiated from surface porosity and un-melted regions beneath the specimen surface. This is due to the fact that crack progression takes more time in LCF, which provides an opportunity for other cracks to initiate. In addition, the defects that act as crack initiation sites in LCF appear to have smaller sizes as compared to those found on the fracture surface of specimens tested in HCF, as can be seen in Figs. 7(b) and (c). This may indicate that the influence of defect size is less pronounced than its distance from the surface in short life regimes. In other words, the fatigue specimens (both conditions) during the long life regime demonstrated internal (i.e. subsurface) crack initiation while the ones in short life regime mostly demonstrated surface crack initiation.

Generally, three main regions that correspond to fatigue crack initiation, fatigue crack growth, and final fracture can be observed on all fatigue fracture surfaces. The fraction of areas of crack propagation and final fracture depend on the applied strain level. Lower applied strains (i.e. long life regimes) result in a large stable crack propagation area, as shown in Fig. 6(a). On the other hand, for higher strain levels (i.e. short life regimes), the crack will not be able to grow very long before final fracture, resulting in a smaller crack growth area, as seen in Fig. 7(a). Similar crack initiation site and morphology of fracture surface were also observed for heat treated fatigue specimens in both LCF and HCF. Voids and un-melted powder (attributed to entrapped gas in melt pool and lack of melting during fabrication, respectively) can be seen along the final fracture surface of specimens in both as-built and heat treated conditions.

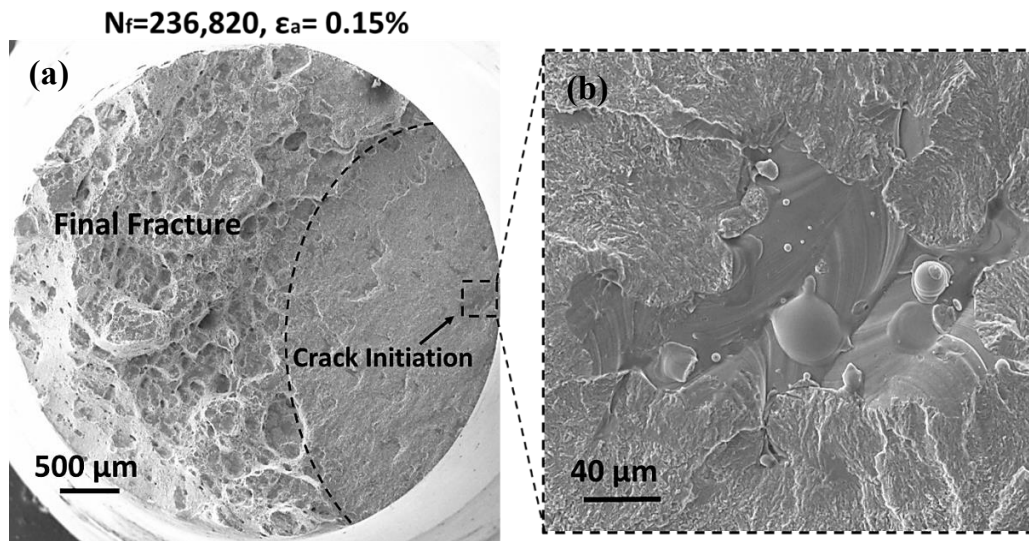


Figure 6. (a) An overall view of fracture surfaces for as-built SLM 17-4 PH SS at low strain 0.15% ($N_f=236,820$) and (b) a magnified view of the crack initiation site indicating that fatigue cracks initiated from an un-melted region close to the surface.

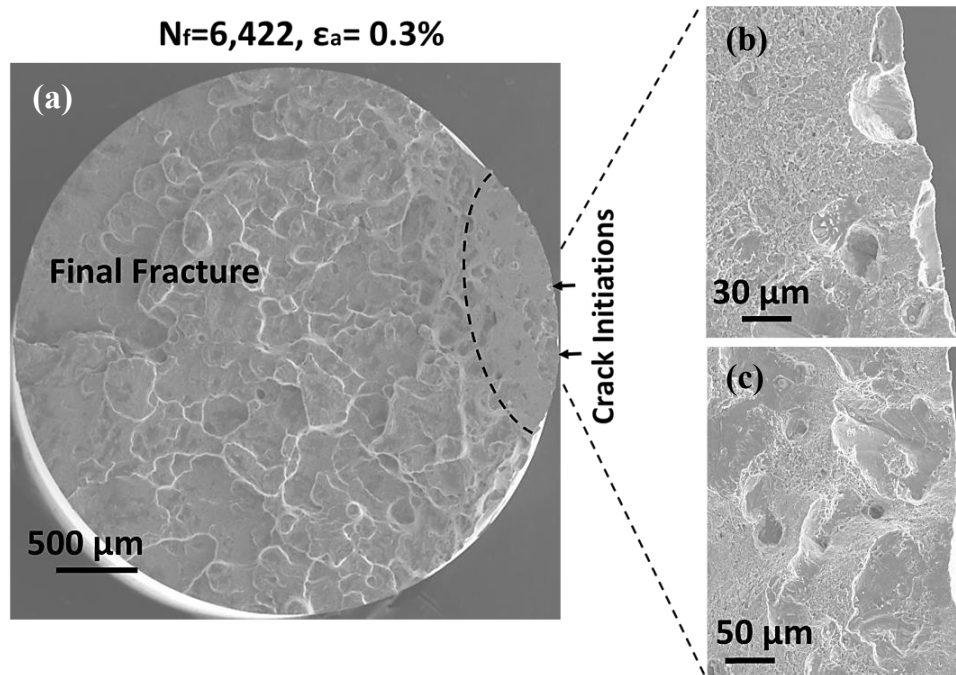


Figure 7. (a) An overall view of fracture surfaces for as-built SLM 17-4 PH SS at strain amplitude of 0.3% ($N_f=6,422$), and a magnified view of the crack initiation sites including (b) pores beneath the specimen surface and (c) an un-melted region close to the surface.

Conclusions

In this study, the fatigue behavior of 17-4 PH stainless steel fabricated via SLM in both the as-built and heat treated (solution annealing and aging) conditions was investigated. A strain-controlled uniaxial test setup with a strain-ratio of $R = -1$ (fully-reversed) was employed. The following conclusions can be drawn based on the experimental results:

1. Defects inherent to powder-based AM has a substantial effect on fatigue life, especially in long life regimes. Unexpectedly, HCF lives of heat treated SLM specimens were lower than their as-built counterparts. This may be explained by heat treatment hardening 17-4 PH SS, making the material more sensitive to impurities.
2. Fatigue strength of heat treated SLM 17-4 PH SS was found to be significantly lower than wrought material in the H1050 condition. Aside from differences in microstructure, the presence of defects, including pores and un-melted regions/powder, were the main contributors for the shorter fatigue life of SLM 17-4 PH SS.
3. The fatigue strengths of the investigated SLM 17-4 PH SS specimens were found to be lower than those measured from 17-4 PH SS made using a similar AM processing technique. This may be explained by differences in the employed fatigue test setup (i.e. rotating bending versus closed loop uniaxial) and/or the design (i.e. building orientation) and process parameters utilized.
4. Fracture surfaces of fatigue specimens revealed that cracks were mostly initiated from un-melted regions that formed due to insufficient fusion, and pores, which may have formed via entrapped gas. Cracks initiated from large un-melted regions adjacent to the surface of specimens failed under high strain amplitude (i.e. long life regime). Multiple crack initiation sites on the surface were observed for specimens tested in shorter life regime.

References

- [1] S.M. Thompson, L. Bian, N. Shamsaei, A. Yadollahi, An Overview of Direct Laser Deposition for Additive Manufacturing; Part I: Transport Phenomena, Modeling, and Diagnostics, Submitt. to Addit. Manuf.
- [2] A. Yadollahi, D. Seely, N. Shamsaei, S.M. Thompson, Effects of Process Time Interval and Heat Treatment on the Mechanical and Microstructural Properties of Direct Laser Deposited 316L Stainless Steel, Submitt. to Mater. Sci. Eng. A.
- [3] N. Shamsaei, A. Yadollahi, L. Bian, S.M. Thompson, An Overview of Direct Laser Deposition for Additive Manufacturing; Part II: Mechanical Behavior, Process Parameter Optimization and Control, Submitt. to Addit. Manuf.
- [4] J. Hunt, F. Derguti, I. Todd, Selection of Steels Suitable for Additive Layer Manufacturing, Ironmak. Steelmak. 41 (2014) 254–256.
- [5] J. Wu, C. Lin, Tensile and Fatigue Properties of 17-4 PH Stainless Steel at High Temperatures, Metall. Mater. Trans. A. 33 (2002) 1715–1724.

- [6] L.E. Murr, E. Martinez, J. Hernandez, S. Collins, K.N. Amato, S.M. Gaytan, et al., Microstructures and Properties of 17-4 PH Stainless Steel Fabricated by Selective Laser Melting, *J. Mater. Res. Technol.* 1 (2012) 167–177.
- [7] X. Lin, Y. Cao, X. Wu, H. Yang, J. Chen, W. Huang, Microstructure and Mechanical Properties of Laser Forming Repaired 17-4PH Stainless Steel, *Mater. Sci. Eng. A.* 553 (2012) 80–88.
- [8] H.K. Rafi, D. Pal, N. Patil, T.L. Starr, B.E. Stucker, Microstructure and Mechanical Behavior of 17-4 Precipitation Hardenable Steel Processed by Selective Laser Melting, *J. Mater. Eng. Perform.* 23 (2014) 4421–4428.
- [9] W.E. Luecke, J.A. Slotwinski, Stainless Steel Made by Additive Manufacturing, *J. Res. Natl. Inst. Stand. Technol.* 119 (2014) 398–418.
- [10] J.T. Sehart, G. Witt, Dynamic Strength and Fracture Toughness Analysis of Beam Melted Parts, *Proc. 36th Int. MATADOR Conf.* Springer London., 2010: pp. 385–388.
- [11] A. Yadollahi, N. Shamsaei, S.M. Thompson, A. Elwany, L. Bian, Mechanical and Microstructural Properties of Selective Laser Melted 17-4 PH Stainless Steel, in: ASME, 2015.
- [12] H.A. Stoffregen, K. Butterweck, Eberhard Abele, Fatigue Analysis in Selective Laser Melting: Review and Investigation of Thin-Walled Actuator Housings, in: *Solid Free Fabr. Symp.*, 2013: pp. 635–650.
- [13] A. Aboutaleb, L. Bian, S.M. Thompson, N. Shamsaei, A. Elwany, Designing Laser-Based Additive Manufacturing Experiments Using Adaptive Minimum Energy Design, in: *ISERC Conf. Expo*, Nashville, TN, 2015.
- [14] ASTM Standard, ASTM E 606-12 - Standard Practice for Strain-Controlled Fatigue Testing, (2012).
- [15] J. Wu, C. Lin, Influence of Frequency on High-Temperature Fatigue Behavior of 17-4 PH Stainless Steels, *Mater. Trans.* 44 (2003) 713–721.
- [16] ASM Handbook, ASM Handbook Volume 4, Heat Treating., Mater. Park. OH ASM Int. (1991).
- [17] N. Shamsaei, a. Fatemi, Effect of Hardness on Multiaxial Fatigue Behaviour and Some Simple Approximations for steels, *Fatigue Fract. Eng. Mater. Struct.* 32 (2009) 631–646.
- [18] R.I. Stephens, A. Fatemi, R.R. Stephens, H.O. Fuchs, *Metal Fatigue in Engineering*, 2nd Edition, Wiley. (2000).
- [19] H.A. Leybold, Axial-Load Fatigue Tests on 17-7 PH Stainless Steel Under Constant-Amplitude Loading, NASA Tech. Note 19980228273 (1960).